Accepted article.

Design and Assessment of a Single-size Semi-soft Assistive Mitten for People with Cervical Spinal Cord Injuries

Daisuke Kaneishi[1], Jessica EnShiuan Leu[1], Julia O'Donnell[1], Campbell Affleck[2], Robert Peter Matthew[3], Andrew McPherson[4], Masayoshi Tomizuka[1], and Hannah S. Stuart[1]

***Abstract*— Assistive orthotics have the potential to augment the grasping capabilities of individuals with limited hand functionality. People with a cervical-level spinal cord injury (SCI) lack direct control of semi-flaccid, curled fingers on both hands, which often precludes independent donning and doffing of orthotics, thus limiting their use in daily life. This paper presents a novel orthotic designed to improve hand functionality while facilitating independent daily use for individuals with cervical SCI: the Single-size Semi-soft Assistive Mitten (SSAM). This device utilizes a slim dorsal leaf spring and underactuated cable drive to passively open and actively close the hand, in a way that is robust to variations in hand size. This mitten is intended to improve ease of donning and doffing, as the device is attached to all fingers at once. A prototype is developed based on simulation studies, and grasping performance of the proposed design is validated with five healthy subjects. Successful grasping trials, along with positive user feedback, suggest that the SSAM has a comfortable and intuitive design for long-term, independent use and will enable future studies into feasibility of daily use for people with SCI.**

I. INTRODUCTION

A. Background of Spinal Cord Injuries

Around 300,000 individuals with spinal cord injury (SCI) live in the United States, and there are more than 8,000 annual incidences of SCI at the cervical level every year [1]. Damage to the spinal cord at C6 or C7 manifests as tetraplegia (quadriplegia), with loss of sensory and motor function including in the hands and arms [2]. Typical muscular effects for complete C6/C7 SCI include loss of active control of the fingers, triceps (elbow extension), and torso and below, while biceps function (elbow flexion) and wrist supination and extension remain strong. Muscle shrinkage during atrophy provides restorative force in the fingers, which many affected individuals use to manipulate lightweight objects through tenodesis[1] without an orthosis [3], [4], [5]. This restorative force causes the fingers to curl inwards into the hand, with a typical resting position of fingers lightly touching the palm, although it is possible to manipulate the fingers passively with nearly full range of motion [2]. Thus, depending on the wrist position and stiffness of the fingers, the use of another hand or an object is often required to extend the fingers prior to grasping through tenodesis. People with cervical SCI often desire a stronger prehensile grasp to improve quality of life [6]. A device which enables active hand opening and closing could assist in activities of daily living (ADL).

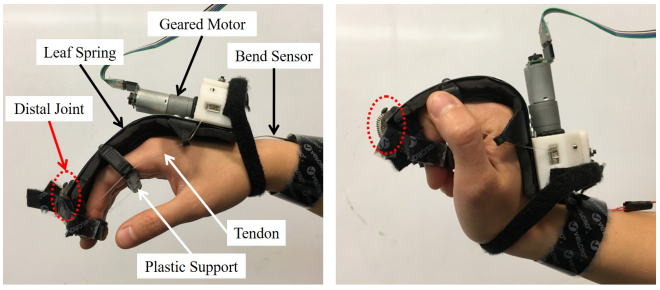

Fig. 1. Primary features of the SSAM on a relaxed human hand. During wrist extension, the bend sensor triggers mechanism/hand closing, actuated by the geared motor and tendon. The leaf spring motion largely contributes to MCP joint flexing, while the distal joint amplifies flexing at the PIP and DIP joints. This semi-soft design fits a variety of hand sizes, and the plastic support is designed for donning without necessitating fine finger control.

B. Related Work

A broad range of assistive technologies have been designed to restore lost hand functions, like wearable devices and exoskeletons. Some passive devices mechanically transmit forces provided by the user (e.g., using wrist extension to close the fingers as in [7], [8]). Active devices can potentially restore multiple hand functions (e.g., pinch, lateral pinch, and grip) for users with cervical SCI or after-effects of stroke [9], [10] by implementing external actuators and transmission systems [11], [12].

Rigid external skeletal frames are traditionally utilized in these active devices to transmit assistive forces efficiently to each finger joint. The stiffness of such materials makes for simple kinematic models. However, for comfortable and efficient operation, the device must be well-aligned with the human joints, which necessitates custom fitting for most users, constrains natural motion, and requires an explicit (often heavy) joint for each degree of freedom [9]. Recent studies have introduced soft robotic approaches using deformable materials, such as cable-driven textiles, leaf springs, and inflatables, alone or in combination with a rigid skeletal

[1] Authors are with the Department of Mechanical Engineering, University of California, Berkeley, CA 94720, USA, {kaneishi, jess.leu24, julia_odonnell, tomizuka, hstuart}@berkeley.edu

[2] C. Affleck is with the Department of Computer Science, University of California, Berkeley, CA 94720, USA, cbaffleck@berkeley.edu

[3] R.P. Matthew is with the Department of Electrical Engineering and Computer Science, University of California, Berkeley, CA 94720, USA, rpmatthew@berkeley.edu

[4] A. McPherson is with the Jacobs Institute for Design Innovation and the Embodied Dexterity Group, University of California, Berkeley, CA 94720, USA, drewmcpherson25@berkeley.edu

[1]Tenodesis, the passive closing of the hand upon wrist extension and opening upon wrist flexion, is an established means for people with cervical SCI to lightly grasp objects, and has been augmented with mechanical devices such as the *tenodesis hand splint*.

frame, as in [13], [14]. These underactuated devices (wherein the number of actuators is less than the number of effective joints) can closely mimic natural human hand motion [5], [15]. Accordingly, these devices have the potential to circumvent joint misalignment [16] and to improve the design aesthetic [17]. Analysis such as finite element method [16] is essential to simulate large-deformation, compliant devices.

While an assistive device may be fitted by a researcher in the laboratory, to be useful for ADL the intended user must have confidence in their ability to independently don and doff such a device. Assistive gloves with five fingers [13], [14], [16] may be useful for patients with hemiplegia, as they can attach the glove using the unaffected hand; however, this may be difficult or nearly impossible for individuals with loss of motor function in both hands, such as with C6/C7 SCI. Finger flaccidity and resting palm-curled finger position which result from a cervical SCI further compromise donning of soft materials, such as a traditional fingered glove. An assistive device suited for people with C6/C7 SCI must be specially designed for independent donning and doffing, for support to both open and close the hand, and for low risk of joint misalignment between the user and the device.

C. Objectives

This paper introduces an orthotic design, the Single-size Semi-soft Assistive Mitten (SSAM, Fig. 1), for an individual with C6/C7 SCI to facilitate independent donning/doffing as well as grasping and object manipulation. The leaf spring curves across the entirety of the dorsal part of the hand, which enables the device to control the finger joints irrespective of hand size and specific joint locations. Simulation of the leaf spring as a cantilever beam reveals the utility of an additional distal joint to further close the fingers for a more powerful wrap grasp. We here present a simulation study of this orthotic and experimental validation of an initial prototype with users of varying hand size.

The rest of this paper is organized as follows. Section II explores mathematical modelling and analysis of the leaf spring as well as the additional distal joint, and details a prototype to empirically validate the proposed design concepts and the experimental conditions. Experimental results with healthy human subjects are shown in Section III, and the performance of the SSAM is validated in Section IV. Finally, conclusions are given in Section V.

II. METHOD

We first study the primary component, a leaf spring, acting mainly at the user's metacarpophalangeal joint (MCP) to passively extend the fingers (Fig. 2). We then build upon these results with an additional distal joint, as shown in Fig. 5, which expands the range of motion about the distal and proximal interphalangeal joints (DIP/PIP). Section II-C explains a prototype developed for empirical validation of the proposed design. Section II-D describes the experiential procedures used to validate the models and performance predicted.

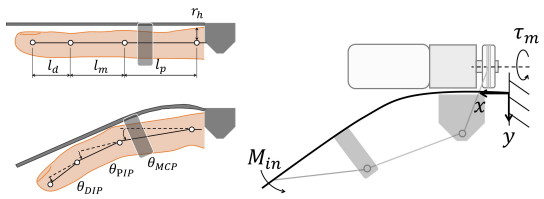

Fig. 2. Finger dimensions, and the relationships between spring-loaded deflection of leaf spring and angles of the DIP, PIP, and MCP joints. Actuators such as an electrical motor apply a spring beam bending moment around an axis vertical to the page surface (i.e., z-axis).

A. Modeling and Analysis of Leaf Spring

Fig. 2 shows our model to simulate the stainless steel leaf spring's influence on the finger joints. We approximate the leaf spring as a two-dimensional cantilever beam extending to the tip of the middle finger (longest finger on the hand), and analyze the elastic deformation under static loading. The axes x, y are defined as proximal-distal and dorsal-palmar directions of the finger respectively, when the finger is extended. Note that we do not necessarily expect that the y axis is aligned parallel to the direction of gravitational force, as the device may be used in different postures (e.g., Fig. 13). A direction of the moment M_{in} produced around the z axis by the loading is defined based on the right-handed coordinate system in Fig. 2(Right).

Considering a constant positive bending moment M_{in} applied to the leaf spring as shown in Fig. 2, the elastic deformation δ of the cantilever in y axis at a distance x from the origin of the coordinate (i.e., the fixed point) can be estimated as follows [18]:

$$M_{in} = G(\tau_m) \tag{1}$$

$$\delta(M_{in}, x) = \frac{M_{in}}{2B}x^2 \tag{2}$$

where τ_m is an input torque from the motor, G is a function relating the motor torque to the applied moment (i.e., M_{in}), and flexural rigidity B is expressed as follows [18]:

$$B = E\frac{bh^3}{12(1-\nu^2)} \tag{3}$$

where E is longitudinal elastic modulus, b is width, h is thickness, and ν is the Poisson ratio of the material. A constraint on total length ($100 \cdot 10^{-3}$ m) is added to (2) such that the effects of elongation are neglected.

Finger curling joint angles were estimated based on geometrical analysis from modeled cantilever deflection of the leaf spring; we neglect finger reaction forces at this time[2]. Accordingly, we assume that the hand is fully open when the leaf spring is at equilibrium (i.e., $\delta = 0$). We model the finger as a series of three zero-mass rigid bodies connected with three zero-impedance pin joints (i.e., DIP, PIP, and MCP), assuming for simplicity that the center of rotation of each finger joint is located at a constant distance r_h below the leaf

[2]MCP stiffness studies of healthy subjects indicate that passive flexing forces may be relatively small [19]. Thus, at this time, we assume that the leaf spring alone will be able to passively extend the fingers of people with SCI, and that finger kinematics can be neglected in this initial study.

TABLE I

SIMULATION PARAMETERS USED TO COMPUTE FIGURE 4

Variable (unit)	Value	Variable (unit)	Value
$E\ (Pa)$	$193 \cdot 10^9$	$\nu\ (-)$	0.3
$b\ (m)$	$80 \cdot 10^{-3}$	$h\ (m)$	$0.25 \cdot 10^{-3}$
$M_{in}\ (Nm)$	*in legend*	$l_d\ (m)$	$27.5 \cdot 10^{-3}$
$l_m\ (m)$	$32.5 \cdot 10^{-3}$	$l_p\ (m)$	$35 \cdot 10^{-3}$

spring as shown in Fig. 2(Left). By setting the skin circle at each joint tangent to the flexed leaf spring, and assuming that there is no friction between the skin and the plate as the hand closes, we numerically compute the coordinates of each joint, and subsequently compute θ_{DIP}, θ_{PIP}, and θ_{MCP}, as defined in Fig. 2. Effective torsional stiffnesses at each joint are defined in our model according to the relation between the moment applied to the leaf spring and corresponding joint displacements as follows:

$$K_i = \frac{M_{in}}{\Delta\theta_i} \quad i \in \{DIP, PIP, MCP\} \tag{4}$$

where $\Delta\theta_i$ is a displacement from the initial angle $\theta_{i_0} = 0$.

Simulation results were computed using the software `Matlab 2016b` and conducted based on (2), using the parameters listed in Table I. These parameters are chosen to reflect steel spring material properties and an average-sized hand. Fig. 3A shows an example simulation result. Three large hollow circles indicate initial coordinates of the finger tip, DIP, PIP, and MCP, connected by dashed lines representing the phalanges, in an extended pose. Black crosses indicate the initial coordinates of the leaf spring at 0.01 m intervals. Small magenta circles represent the position of the flexed leaf spring at 0.01 m intervals, and the four large filled circles represent the finger tip, DIP, PIP, and MCP positions, as flexed by the leaf spring. Red dotted circles with radius r_h represent the skin around each joint.

Fig. 3B shows the pose of three fingers with different lengths when $M_{in} = 1.0\ Nm$. The lengths are defined as a vector $\boldsymbol{l}_j$ as follows:

$$\begin{aligned} \boldsymbol{l}_j &:= [l_d, l_m, l_p]^T,\ j \in \{Nominal, Long, Short\} \\ \boldsymbol{l}_{Long} &= [30, 35, 40]^T \cdot 10^{-3} \\ \boldsymbol{l}_{Short} &= [22.5, 30, 30]^T \cdot 10^{-3} \end{aligned}$$

where l_d, l_m and l_p are the lengths of distal, middle, and proximal phalanges as shown in Fig. 2, respectively. Note that $\boldsymbol{l}_{Nominal}$ is defined in Table I. Fig. 4A shows the leaf spring displacement computed by (2) and the constant-length constraint, at 0.01 m intervals vertically downwards from the flat initial condition, for a range of applied moment M_{in}. Fig. 4B shows the simulated relationship between applied moment and the DIP, PIP, and MCP angles, calculated geometrically by (4), as shown in Fig. 3A.

These simulation results suggest several interesting properties of the leaf spring used for the mitten. Fig. 3B demonstrates that finger flexion by the leaf spring is nearly identical regardless of finger length. In Fig. 4B, approximately linear responses can be found for all joints when applying a small moment ($< 0.2\ Nm$), but nonlinearity is observed for larger

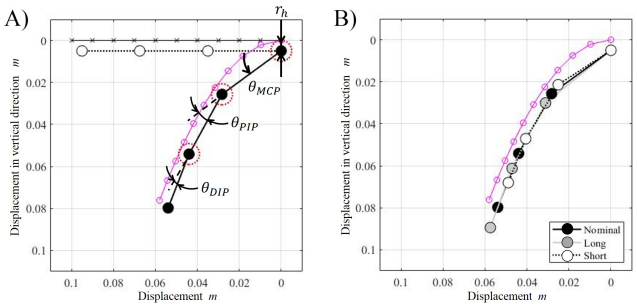

Fig. 3. Modeled bending toward the palm, as in Figure 2: A) Changes of joint angles θ_{DIP}, θ_{PIP}, and θ_{MCP} corresponding to leaf spring displacement at $M_{in} = 1.0$. B) Changes of joint angles for different finger lengths.

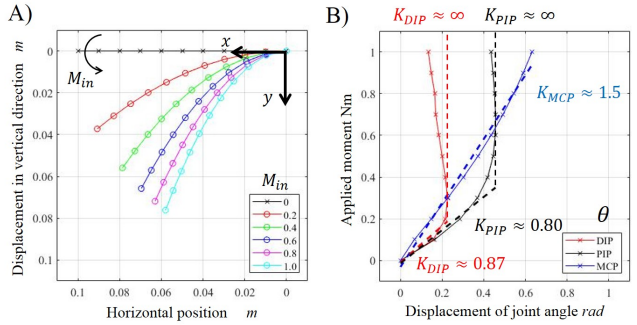

Fig. 4. A) Numerical simulations illustrate the relationship between applied moment M_{in} and displacement δ and B) stiffness properties of the leaf spring.

applied moments, an effect most pronounced at the DIP and PIP joints. These results suggest the following linearized effective spring stiffnesses (Nm/rad) computed based on (4):

$$K_{DIP} \approx \begin{cases} 0.87, & \theta_{DIP} \leq 0.23 \\ \infty, & \theta_{DIP} > 0.23 \end{cases} \tag{5}$$

$$K_{PIP} \approx \begin{cases} 0.80, & \theta_{PIP} \leq 0.45 \\ \infty, & \theta_{PIP} > 0.45 \end{cases} \tag{6}$$

$$K_{MCP} \approx 1.5 \tag{7}$$

Thus, if the moment was exerted on the leaf spring as indicated in Fig. 4A, the model suggests that the leaf spring would deflect primarily at the MCP, a motion typical for precision pinching, with relatively straight fingers.

B. Additional Distal Joint for Enhanced Wrap Grasping

The effective spring stiffnesses K_{DIP}, K_{PIP} demonstrate that the leaf spring limits the range of motion of corresponding joints, due to nonlinearity (Fig. 4B). However, a design which allows actuation of the DIP or PIP can enable wrap grasps [20], a more powerful configuration suitable for extruded objects (e.g., handles), which is possible with limited thumb opposition [21]. Additional distal flexibility is thus desired in the SSAM design, as shown in Fig. 5.

Fig. 5 shows a free body diagram at equilibrium representing the SSAM with both the proximal leaf spring and an additional distal rotational joint with stiffness K_{add}.

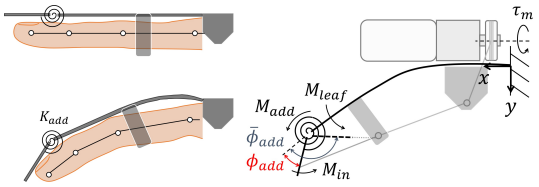

Fig. 5. Proposed distal joint to expand range of DIP/PIP motion (left) and free body diagram of the device with additional distal joint mechanism at equilibrium (right).

This spring may be tuned independently as another design parameter. The parameters in Fig. 5 satisfy the following conditions:

$$M_{leaf} = M_{add} = M_{in} \tag{8}$$

where M_{add} and M_{leaf} are applied moments corresponding to the additional joint and to the leaf spring. Note that, regardless of the pose of the tendon, a constant moment M_{in} is applied in the following simulation study, assuming that the motor is well-controlled based on (1).

Deflection of the system and changes of the DIP, PIP, and MCP angles were estimated once again based on an updated geometrical analysis. First, the leaf spring deflection is computed with the applied moment M_{in} following the condition (8) and the method shown in Fig. 4, for the proximal $70 \cdot 10^{-3}$ m of the device. Next, the effects of the distal joint are modeled as the torsional spring with stiffness K_{add}, assuming attachment as a pin joint to a rigid member coincident with the end of the leaf spring. The distal joint angle ϕ_{add} is determined according to the applied moment M_{in} (i.e., M_{add}) and stiffness K_{add}. Three values of K_{add}, 0.75, 1.5, and 3.0 Nm/rad, are chosen based on K_{MCP} in (7), as the leaf spring deflects primarily at the MCP. The length of the spring steel is now $70 \cdot 10^{-3}$ m to insert the additional mechanism ($L_d = 30 \cdot 10^{-3}$ m). Note that, due to mechanical constraints, we set an upper limit of the distal joint angle $\bar{\phi}_{add}$ at which a transmission cable and the distal component are aligned. This result is validated in Section III.

Fig. 6 shows example simulation results applying two different moments ($M_{in} = 0.4, 0.8$ Nm). The gray-scaled large filled circles represent the results with different spring stiffnesses, $K_{add} = 0.75, 1.5$, and 3.0 Nm/rad. Fig. 7A shows the simulated relationship between the displacement δ and a range of applied moments M_{in}. Fig. 7B shows the simulated relationship between the applied moment and the finger DIP, PIP, and MCP angles. Note that the spring stiffness K_{add} was set to be 0.75 Nm/rad in Fig. 7. More distal flexibility, through the additional joint, increases both DIP and PIP joint ranges of motion to greater than 0.6 rad. The design parameter K_{add} may be tuned relative to the stiffness of the leaf spring K_{MCP} to achieve different curling behaviors. For this particular design, K_{add} is designed smaller than K_{MCP} in order to promote wrap grasping as opposed to pinching.

C. Prototype for Empirical Validation

Hardware was developed based on the simulation results to validate effects of the design through experiments (Fig. 8).

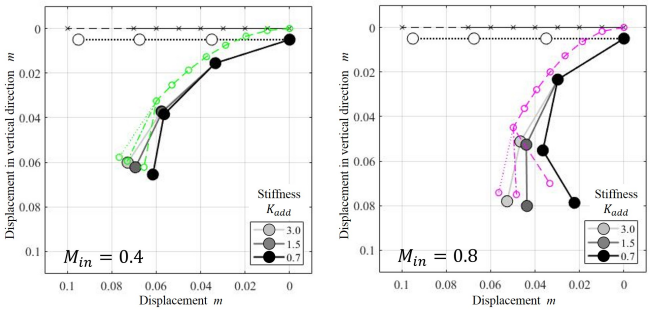

Fig. 6. Changes of joint angles for spring stiffness K_{add}.

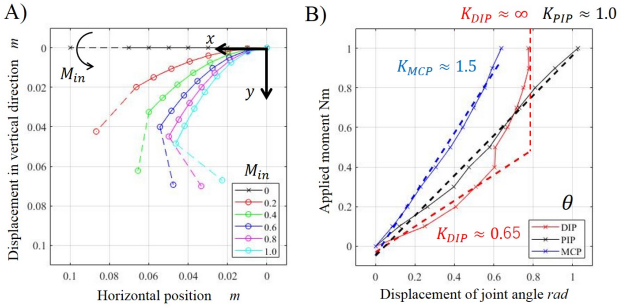

Fig. 7. A) Numerical simulations illustrate the relationship between applied moment M_{in} and displacement δ in y direction and B) stiffness properties of the leaf spring with torsional spring $K_{add} = 0.75$ Nm/rad.

The underactuated mechanism is comprised of a leaf spring, an additional distal joint, and a motorized winch that drives the cable. A detailed description of the proof-of-concept device follows.

1) Leaf Spring: Table II and Fig. 9 show major design parameters to machine the leaf spring. The length L_3 and width W were determined to cover the majority of the dorsal finger surface of a human subject. The thickness t is a trade-off between stiffness and plastic deformation which occurs after moderate use (i.e. the MCP never opens completely to $\theta_{MCP} = 0$). After testing several different configurations, we used two layers of sheet metal of 0.18 mm thickness to achieve an acceptable neutral hand position. A foam pad (thickness ≈ 4 mm) was inserted between the hand and the leaf spring to reduce contact pressure for user comfort.

To minimize the effort for donning, there is only a single attachment for all four fingers, and the thumb is excluded. A single hard plastic loop attached to the leaf spring fits around all four proximal phalanges on the palmar side. This rigid component is designed to facilitate independent donning, such that a person with flaccid fingers could passively hook their fingertips onto the support, before sliding their hand into the leaf spring mitten. This minimalist design also leaves a large amount of the user's palmar skin exposed, which enables the concurrent use of commercial palm gloves with thumb loop design to assist thumb (Fig. 8). The device is further secured to the user's hand with flexible hook-and-loop straps around the distal phalanges and wrist.

2) Distal joint mechanism: Inspired by the Ocean One robot hand design [20], we designed a flexible distal joint

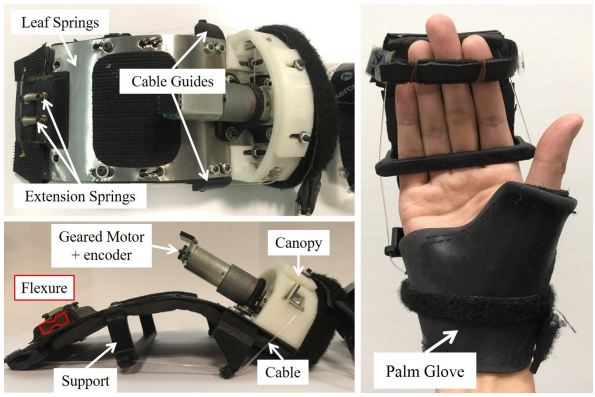

Fig. 8. The details of the final mechanism design include: a winch canopy with dowel pins; cable guides for routing; a U-shaped rigid finger support; a geared motor with encoder; hinged design at the distal joint made up of rubber flexures and extension springs; the leaf spring steel sheets.

which consists of a 3D printed housing, two compliant urethane flexures (cast with Smooth-on PMC 780, with Young's modulus of approximately 2.76 MPa), and two extension springs (stiffness 0.958 N/mm) in parallel. The parallel spring-flexure design allows for more compliance out of the plane of the leaf spring, to couple closer with the natural human PIP motion.

An equivalent torsional spring constant of the two extension springs K_{add} acting about the DIP may be estimated based on (4) by computing a moment produced by the extension springs corresponding to given displacements of the joint angle. The torsional spring constant for our dual-spring joint design was estimated to be 0.1 Nm/rad based on empirical data obtained from a similar joint design (the proximal joint in the Ocean One finger [20]).

3) Cable-driven Actuation Mechanism: A geared DC motor (gear ratio 156:1, Pololu 3492) was installed on the dorsal-proximal side of the leaf spring. This motor provides torque sufficient to close the hand (nominal maximum torque of 0.92 Nm, resulting in max. 46 N of cable tension with a $\phi 20$ mm pulley) in a small package ($20D \times 44L$ mm, 46 g). A relative-position magnetic encoder (Pololu 3499, 20 counts/rev) was installed on the motor shaft to measure and estimate position θ_m and its velocity $\dot{\theta}_m$. Note that different actuators could be selected to further reduce size and weight of the overall design.

A nylon cable (0.71 mm diameter, McMaster-Carr 9442T4) is connected to the motor via a winch (20 mm diameter, aluminum alloy, MiSUMi MBRDAC20-1-4), and both ends of the cable are knotted to the pulley. Two 3D printed (ABS) cable guides are attached to the leaf spring to route the cable, and a 3D printed (ABS) canopy with dowel pin fixed-pulleys prevents the cable from jumping off the winch while reducing tendon friction and wear.

4) Control System: The SSAM is designed for intuitive operation to mimic tenodesis by tracking the wrist motion [5], closing the hand upon wrist extension and opening upon wrist flexion. Fig. 10 shows an overview of the active control system to assist the user with grasping through the proposed design. The controller is designed as a finite state

TABLE II

EMPIRICAL MEASUREMENTS OF DEVICE DESIGN PARAMETERS

Variable (unit)	Value	Variable (unit)	Value
L_d (m)	$20 \cdot 10^{-3}$	L_1 (m)	$80 \cdot 10^{-3}$
L_2 (m)	$145 \cdot 10^{-3}$	L_3 (m)	$185 \cdot 10^{-3}$
W (m)	$80 \cdot 10^{-3}$	t (m)	$4 \cdot 10^{-4}$

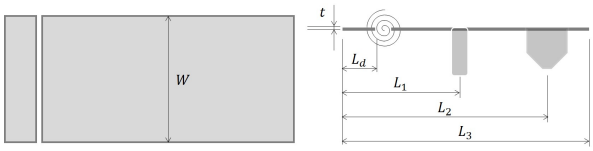

Fig. 9. Dimensions of a prototype in Fig. 8. A grey rectangular and black polygons indicate a leaf spring and 3D printed supports, respectively. A swirl indicates a flexure modelled as a torsional spring.

machine (FSM) which utilizes hysteresis control to prevent from chatterings between Open and Close state [22].

There are three inputs to the controller: a binary signal sig, θ_m, and $\dot{\theta}_m$. The binary signal is designed as a guard condition to switch from Neutral to Close state or from Grasp to Open state in Fig. 10, i.e., turning on the actuator. The binary signal is defined as follows:

$$sig = \begin{cases} 0, & y(t) < \underline{\eta} \\ 1, & y(t) > \overline{\eta} \end{cases} \tag{9}$$

where $y(t)$ is a sensor measurement, and $\underline{\eta}$, $\overline{\eta} \in \mathbb{R}$ are constants tuned for each user. A short bend sensor (Adafruit, 1070) was utilized to detect the user's wrist motion (Fig. 1). The sensor was fixed to the proximal edge of the leaf spring, near the wrist, and its position was adjusted to fit the user with a hook-and-loop strap.

The angular inputs θ_m and $\dot{\theta}_m$ in Fig. 10 are measured by the encoder and utilized to control the geared motor with a constant input C (i.e., constant voltage inputs). Note that transient response is neglected in this study, as we focused on steady state response in simulation study in section II. The control input u can be designed as feedback controller, such as PID control, to achieve comfortable interaction through further system identification process. $\underline{\theta}_m$ and $\overline{\theta}_m$ are reference positions for the actuator as the angular position thresholds to enable transitions from Close to Grasp and Open to Neutral states, respectively. An additional guard for the transition from Close to Grasp states, in terms of the velocity threshold ε, is introduced to detect motor stall when grasping an object.

A microcontroller (Arduino UNO) measures the bend sensor, creating the binary signal with (9). The microcontroller controls the motor through a motor driver (Dual MAX14870, Pololu), generating a command u to the motor based on the signals shown in Fig. 10.

D. Experimental Conditions

We conducted three experiments to verify the proposed design functionality and its performance with human subjects. The first experiment was conducted to confirm closing performance of the proposed design with and without a subject. Two setups were chosen and compared: a full leaf

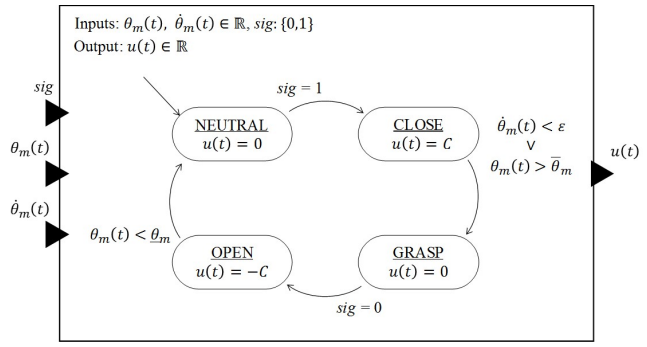

Fig. 10. Finite state machine which controls the proposed device.

spring mitten (without the additional distal joint), and the device with the additional distal joint. The experiment was performed with leaf springs of equal total thickness, and the overall length and width of both devices were also the same, as shown in Table II. The device was fixed to a rigid base, and we manually tuned control inputs to the motor and examined the corresponding steady-state curvatures of the step response. The duty cycle of the PWM input signal (i.e., the constant input C in Fig. 10) was set to be a constant at 35% in this experiment, which produced around 4.2 Nm estimated as the moment M_{in} applied to the leaf spring.

The goal for the second and third experiments is to test the grasping force and the functional performance with human subjects. In these experiments, five healthy individuals (three males, two females, all right handed) were recruited under informed consent, which was approved by the Institutional Review Board of University of California, Berkeley (IRB: 2012-12-4872). Before the experiments, hand sizes of the subjects were recorded. Length of distal, middle, and proximal phalanges of the third fingers were 26 ± 4, 32 ± 2, and 34 ± 5 mm, respectively. Distance between the second and forth fingers at MCP (i.e., width of hands) was 94 ± 12 mm.

In the second experiment, the subjects were asked to sit on a chair and wear the mitten. All the subjects were asked not to actively control their hands after wearing the mitten to simulate the situation of individuals with C6/C7-SCI. The peak and steady-state grasping forces produced by the mitten were measured with a digital hand dynamometer (CAMRY) for three trials (Figure 11, Left) while we actively closed the mitten, independent of wrist motion. The duty cycle of the PWM motor input signal was set to 70% in all human experiments.

Before the third experiment, subjects received an oral explanation of the mitten's FSM functions as shown in Figure 10. After the subjects spent a few minutes familiarizing themselves with the device, they were asked to perform grasping tasks by themselves with the mitten. As shown in Figure 11(Right), there were four different stiffness/shapes of objects, balls (racquet, tennis) and bottles (cylinder, cone). Subjects were instructed to grasp, lift, and release each object in succession. Feedback was collected from all subjects whether the assistive mitten was (i) comfortable, (ii) easy to wear, and (iii) if it could provide sufficient force to achieve the given tasks. These three elements were evaluated on a scale of 1 (worst) to 5 (best).

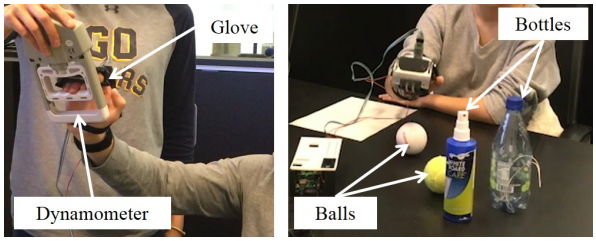

Fig. 11. Experimental setups for the second and third experiments.

III. RESULTS & ANALYSIS

Fig. 12 shows the free-bending curvature experiments. Figure 12A and B show steady state responses to step inputs of the device with only the leaf spring and with the additional joint mechanism, respectively. Fig. 12(Left) demonstrates the different effects on the DIP/PIP joints when worn on a hand. Strips of white tape delineate the position of the flexed leaf spring at 0.01 m intervals. Fig. 12(Center) indicates the effects of additional joint mechanism under the same condition in left figure except the hand. Yellow crosses represent positions of the white tapes, which were identified as middle points of short sides close to the leaf spring. Edges of the strips were detected with *edge* function in `Matlab 2018b`, which can be confirmed in Fig. 12(Right). Fig. 12(Right) shows differences between the experimental results (yellow crosses) and simulation results (white, green circles when $M_{in} = 0, 4.2$ Nm) conducted under the identical conditions except design parameters (i.e., Table I and II). Simulation results were superimposed on Fig. 12(Center), assuming that the proximal (i.e., rightmost) point was the origin of coordinates.

A similarity ratio was defined as Euclidean distance to compare the proposed model with the prototype:

$$D_{m,n} = \sum_{i=m}^{n} d(\mathbf{p}_i, \mathbf{q}_i) \tag{10}$$

$$d(\mathbf{p}_i, \mathbf{q}_i) = \sqrt{(p_{i_x} - q_{i_x})^2 + (p_{i_y} - q_{i_y})^2} \tag{11}$$

where i numerates the markers (the yellow crosses and the green circles) starting from the fix base and $\mathbf{p}_i, \mathbf{q}_i \in \mathbb{R}^2$ are the coordinates of the i^{th} marker obtained from simulation and experiments, respectively. Note that the order was defined from the proximal to the distal plots. Three distances were computed from Fig. 12(Right) for the two models as follows:

$$A)\ D_{1,13} = 0.16,\ D_{1,6} = 0.02,\ D_{6,13} = 0.14 \tag{12}$$

$$B)\ D_{1,13} = 0.11,\ D_{1,6} = 0.03,\ D_{6,13} = 0.09 \tag{13}$$

Note that all the units of the ratios are m.

In the grasping force experiment, the peak and steady-state grasping force measured was 20 ± 5 and 14 ± 3 N, respectively. In the object grasping experiment, Fig. 13 shows a sequence of motion keyframes during grasping a racquet ball (top) and a cone-shaped bottle (bottom). Nearly all subjects successfully grasped all objects, with the exception of one cylinder bottle grasp (19 out of 20 trials were successful).

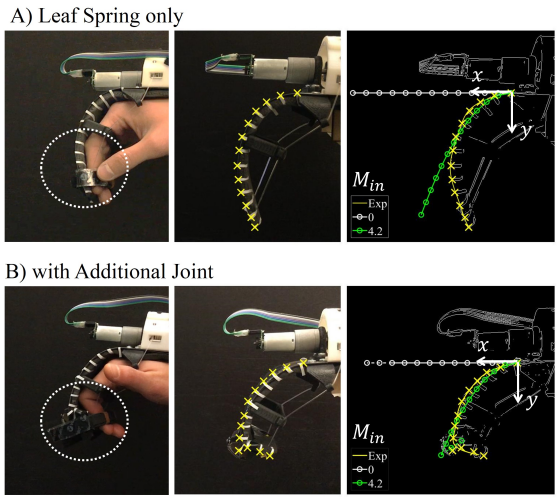

Fig. 12. Differences of orthotic bending curvature A) without and B) with a distal joint. Left and middle images show curvature response in steady states with and without a subject. Right images superimpose corresponding simulation results to the middle.

The subjects reported the device was comfortable and easy to wear (4.2 ± 0.8 and 4.0 ± 0.7) and most felt it provides enough force for grasping (4.4 ± 0.9).

IV. DISCUSSION

A. Validation of Proposed Models

The leaf spring is modelled as a two-dimensional cantilever, and demonstrated DIP/PIP range of motion improvement with the addition of a distal joint, as theoretically shown in Fig. 4B and 7B. In the free-bending test, we validated these proposed model with a prototype. Fig. 12(Center) shows steady-state curvatures of the prototype without and with the additional joint. Fig. 12(Right) superimposes the simulation results, respectively. We validated the proposed models by investigating similarities between these curvatures of experimental and numerical results.

The similarity ratio $D_{m,n}$ indicates the distance between the two curvatures. The mean values of $D_{1,13}$ in (12) and (13) suggest that there were position errors around 1 *cm* at each plots regardless of the additional joint. To be precise, the ratios $D_{1,6}$ in (12) and (13) were much smaller than $D_{6,13}$, as suggested in Fig. 12(Right). One of the reasons being that there was a single hard plastic loop attached to the leaf spring at the 6^{th} plots as shown in the figures and Table II. This U-shaped support might influence force transmission mechanism, compelling the leaf spring, especially its distal part, not to follow the dynamics in (2). In addition, our model assumes that the actuation applied by the tendon is a pure moment, however the significant tension in the tendon may act to buckle the spring steel, resulting in more curvature. Interactions between the leaf spring and the attachments need to be further considered to improve the design and control.

B. Utility of Distal Joint in Grasping Performance

Simulation results motivated the additional mechanism allowing actuation of the DIP/PIP to enable a wrap grasp.

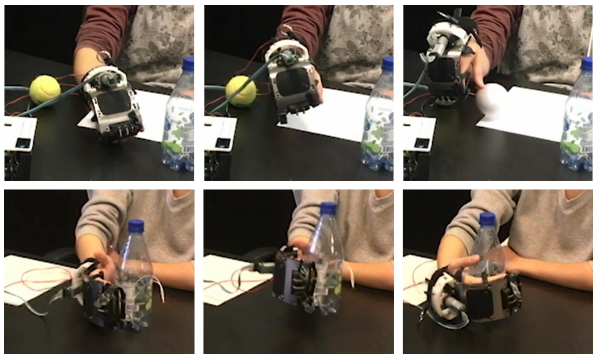

Fig. 13. Grasping a racquet ball (top) and a cone-shaped bottle (bottom) by controlling the assistive device with wrist extension.

Fig. 12A(Left) shows the actual configuration of the hand without the additional joint, which may enable the user to manipulate objects through a pinch grasp, with adequate thumb support. As demonstrated in both simulation and prototype experiments, the leaf spring alone cannot flex the DIP/PIP, following the highly nonlinear stiffness of the effective DIP/PIP model. By adding the distal joint, the DIP/PIP range of motions were improved, which were suitable for a power grasp as suggested in Fig. 12B(Left). Note that the position of the distal joint relative to the users' hand may vary based on their comfort and desired behavior as the device is not fixed firmly to the users' hands. We may conclude that this additional mechanism helps the subject to close their hand into a loose fist as shown in Fig. 1(Right), despite variations in hand size, which all subjects reported was comfortable (ave. score: 4.2).

C. Validation of Grasping Performance as Assistive Device

The mitten was measured with a hand dynamometer to produce stationary grasping force of 14 ± 3 *N*. Although this value is smaller than the grip produced by a healthy subject (> 196 *N*), it was sufficient to grasp balls and bottles (~ 200 *g*) used in this study (Fig. 13), which are representative of typical daily objects. All the subjects felt the mitten could provide enough force for grasping (ave. 4.5) accordingly.

In the grasping experiment, different subjects chose to grasp objects from different directions. In order to observe whether the device will restrict the subject's movement, we did not specify the way to approach each object. Instead, subjects were allowed to choose their preferred method to approach the object and to close the mitten by triggering with wrist extension. For example, some subjects held a racquet ball from the top, while some subjects grabbed a bottle from the side (Fig. 13). Regardless of approach direction, our mitten held objects steadily until the subjects flexed their wrist to open the hand. The mitten design assisted these subjects to grasp with high success rate while allowing the user sufficient freedom of movement.

D. Design for Donning and Doffing

The intuitive design of a single solid plastic support attached to the leaf spring could facilitate donning by hooking the subjects' fingers through the support. All subjects stated

that the device was easy to don and doff (scored ave. 4.0). This proposed design, based on a leaf spring with a compliant joint and a solid plastic support, provided adequate control of the subjects' fingers in order to perform selected grasping tasks of daily living. These results suggest that the SSAM is a valid potential solution for enhancing grasping and performances of object manipulation.

E. Limitation and Future Work

We acknowledge several limitations in this study, as the performance was evaluated only with healthy subjects in the experiments. First, the qualitative experience of healthy subjects may differ from that of a user with SCI. While healthy subjects demonstrated and reported easy donning and doffing of the SSAM, testing with users with SCI is necessary to validate the design for independent use. Furthermore, although instructed to relax the hand and passively wear the orthosis, healthy subjects may have inadvertently contributed to the observed grasping performance of the device. Finally, finger joint stiffness of individuals with SCI may differ from that of healthy subjects [19], which may compromise the performance of the SSAM to passively open the hand. As a future work, we plan to study performance of the SSAM with individuals with SCI while investigating suitable control interfaces [23].

V. CONCLUSIONS

The Single-size Semi-soft Assistive Mitten (SSAM) is intended to facilitate independent donning/doffing as well as improved hand functionality for individuals with C6/C7-SCI. The mitten design with a leaf spring is relatively agnostic to hand size. Simulation studies with the dorsal leaf spring model suggests that distal finger bending via an additional flexure joint is important for wrap grasping. Experimental trials with an initial prototype confirmed the utility of the distal joint, and grasping performance was tested with five healthy subjects. The semi-soft underactuated design with leaf spring and distal joint of the SSAM allowed the subjects to grasp objects comfortably regardless of variation in subject hand size. Future work will study the ability of people with SCI to don, operate and doff SSAM effectively.

ACKNOWLEDGMENT

The authors acknowledge Skye Parker, Monica Li and Kim Euiyoung for helpful conversations on theoretical and design concepts. This material is based upon work supported in part by the University of California Berkeley, Funai Foundation for Infomation Technology, and NSF grant #1362172. Any opinions, findings, and conclusions or recommendations expressed in this material are those of the authors and do not necessarily reflect the views of the funding agencies.

REFERENCES

[1] National Spinal Cord Injury Statistical Center (NSCISC). (retrieved: June 2019) Facts and figures – complete archives. [Online]. Available: https://www.nscisc.uab.edu/

[2] L. Harvey, J. Batty, R. Jones, and J. Crosbie, "Hand function of c6 and c7 tetraplegics 1–16 years following injury," *Spinal Cord*, vol. 39, no. 1, p. 37, 2001.

[3] J. N. Wilson, "Providing automatic grasp by flexor tenodesis," *J. of Joint and Bone Surgery*, vol. 38, no. 5, pp. 1019–1024, 1956.

[4] M. E. Johanson and W. M. Murray, "The unoperated hand: the role of passive forces in hand function after tetraplegia," *Hand Clinics*, vol. 18, pp. 391–398, 2002.

[5] H. In, B. B. Kang, M. Sin, and K.-J. Cho, "Exo-glove: a wearable robot for the hand with a soft tendon routing system," *IEEE Robotics & Automation Magazine*, vol. 22, no. 1, pp. 97–105, 2015.

[6] G. Snoek, M. Ijzerman, H. J. Hermens, D. Maxwell, and F. Biering-Sorensen, "Survey of the needs of patients with spinal cord injury: impact and priority for improvement in hand function in tetraplegics," *Spinal Cord*, vol. 42, no. 9, pp. 526–532, 2004.

[7] Y.-S. Kang, Y.-G. Park, B.-S. Lee, and H.-S. Park, "Biomechanical evaluation of wrist-driven flexor hinge orthosis in persons with spinal cord injury," *J. of Rehabilitation Research and Development*, vol. 50, no. 8, pp. 1129–1138, 2013.

[8] A. A. Portnova, G. Mukherjee, K. M. Peters, A. Yamane, and K. M. Steele, "Design of a 3d-printed, open-source wrist-driven orthosis for individuals with spinal cord injury," *PloS one*, vol. 13, no. 2, p. e0193106, 2018.

[9] Y. Yun, S. Dancausse, P. Esmatloo, A. Serrato, C. A. Merring, P. Agarwal, and A. D. Deshpande, "Maestro: An emg-driven assistive hand exoskeleton for spinal cord injury patients," in *Proc. IEEE Int. Conf. on Robotics and Automation (ICRA)*, May 2017, pp. 2904–2910.

[10] H. K. Yap, J. H. Lim, F. Nasrallah, and C.-H. Yeow, "Design and preliminary feasibility study of a soft robotic glove for hand function assistance in stroke survivors," *Frontiers in Neuroscience*, vol. 11, p. 547, 2017. [Online]. Available: https://www.frontiersin.org/article/10.3389/fnins.2017.00547

[11] B. B. Kang, H. Lee, H. In, U. Jeong, J. Chung, and K. Cho, "Development of a polymer-based tendon-driven wearable robotic hand," in *Proc. IEEE Int. Conf. on Robotics and Automation (ICRA)*, May 2016, pp. 3750–3755.

[12] M. Xiloyannis, L. Cappello, Dinh Binh Khanh, Shih-Cheng Yen, and L. Masia, "Modelling and design of a synergy-based actuator for a tendon-driven soft robotic glove," in *2016 6th IEEE International Conference on Biomedical Robotics and Biomechatronics (BioRob)*, June 2016, pp. 1213–1219.

[13] C. G. Rose and M. K. O'Malley, "Hybrid rigid-soft hand exoskeleton to assist functional dexterity," *IEEE Robotics and Automation Letters*, vol. 4, no. 1, pp. 73–80, Jan 2019.

[14] P. Polygerinos, Z. Wang, K. C. Galloway, R. J. Wood, and C. J. Walsh, "Soft robotic glove for combined assistance and at-home rehabilitation," *Robotics and Autonomous Systems*, vol. 73, pp. 135–143, 2015.

[15] S. Ates, C. J. W. Haarman, and A. H. A. Stienen, "Script passive orthosis: design of interactive hand and wrist exoskeleton for rehabilitation at home after stroke," *Autonomous Robots*, vol. 41, no. 3, pp. 711–723, 2017.

[16] J. Arata, K. Ohmoto, R. Gassert, O. Lambercy, H. Fujimoto, and I. Wada, "A new hand exoskeleton device for rehabilitation using a three-layered sliding spring mechanism," in *2013 IEEE International Conference on Robotics and Automation*, May 2013, pp. 3902–3907.

[17] A. T. Asbeck, S. M. M. D. Rossi, I. Galiana, Y. Ding, and C. J. Walsh, "Stronger, smarter, softer: Next-generation wearable robots," *IEEE Robotics Automation Magazine*, vol. 21, no. 4, pp. 22–33, Dec 2014.

[18] S. Krenk and J. Hgsberg, *Statics and Mechanics of Structures*. Springer, Dordrecht, 2013.

[19] A. Howe, D. Thompson, and V. Wright, "Reference values for metacarpophalangeal joint stiffness in normals," *Annals of the rheumatic diseases*, vol. 44, no. 7, p. 469, 1985.

[20] H. Stuart, S. Wang, O. Khatib, and M. R. Cutkosky, "The ocean one hands: An adaptive design for robust marine manipulation," *The Int. J. of Robotics Research*, vol. 36, no. 2, pp. 150–166, 2017.

[21] M. Cutkosky, "On grasp choice grasp models and the design of hands for manufacturing tasks," *IEEE Trans. on Robotics and Automation*, vol. 5, pp. 269–279, 1989.

[22] E. A. Lee and S. A. Seshia, *Introduction to Embedded Systems, A Cyber-Physical Systems Approach*. MIT Press, 2017.

[23] D. Kaneishi, R. P. Matthew, J. E. Leu, J. ODonnell, B. Zhang, M. Tomizuka, and H. Stuart, "Hybrid control interface of a semi-soft assistive glove for people with spinal cord injuries," in *2019 IEEE 16th International Conference on Rehabilitation Robotics (ICORR)*, June 2019, pp. 132–138.